Observation of Long-Lived Muonic Hydrogen in the 2S State

Randolf Pohl,[1,2,*] Herbert Daniel,[3] F. Joachim Hartmann,[3] Peter Hauser,[2] Franz Kottmann,[1] Valery E. Markushin,[2] Markus Mühlbauer,[3] Claude Petitjean,[2] Wolfgang Schott,[3] David Taqqu,[2] and Peter Wojciechowski-Grosshauser[3]

[1]*Institut für Teilchenphysik, ETH Zürich, 8093 Zürich, Switzerland*

[2]*Paul Scherrer Institut, 5232 Villigen-PSI, Switzerland*

[3]*Physik Department, Technische Universität München, 85748 Garching, Germany*

(Received 14 July 2006; published 9 November 2006)

The kinetic energy distribution of ground state muonic hydrogen atoms $\mu p(1S)$ is determined from time-of-flight spectra measured at 4, 16, and 64 hPa H_2 room-temperature gas. A 0.9 keV component is discovered and attributed to radiationless deexcitation of long-lived $\mu p(2S)$ atoms in collisions with H_2 molecules. The analysis reveals a relative population of about 1%, and a pressure-dependent lifetime (e.g., $30.4^{+21.4}_{-9.7}$ ns at 64 hPa) of the long-lived $\mu p(2S)$ population, equivalent to a $2S$ quench rate in $\mu p(2S) + H_2$ collisions of $4.4^{+2.1}_{-1.8} \times 10^{11}$ s^{-1} at liquid-hydrogen density.

DOI: 10.1103/PhysRevLett.97.193402 PACS numbers: 36.10.Dr, 34.20.Gj

A measurement of the Lamb shift in muonic hydrogen, i.e., the energy difference of 0.2 eV between the $2P$ and $2S$ states of $\mu^- p$ atoms [1–3], is in progress at the Paul Scherrer Institute (PSI), Switzerland [4]. Vacuum polarization shifts the $2S$ levels by 0.2 eV *below* the $2P$ levels; fine and hyperfine splittings of the $n = 2$ levels are much smaller. The finite size effect is 2% of the Lamb shift.

The μp Lamb shift experiment is expected to give a precise value for the root-mean-square charge radius of the proton [5]. Together with recent advances in H-atom spectroscopy [6,7], this leads to a better determination of the Rydberg constant, and to a test of bound-state quantum electrodynamics on a new level of precision [8].

The most important prerequisite for such an experiment, the availability of sufficiently long-lived $\mu p(2S)$ atoms, has so far not been experimentally established. When muons are stopped in H_2 gas, μp atoms are formed at high n levels and then deexcite predominantly to the ground state (''muonic cascade''). A fraction ε_{2S} of a few percent reaches the metastable $2S$ state whose lifetime is, in the absence of collisions, essentially given by the muon lifetime of 2.2 μs.

In a gas, there is collisional $2S$ quenching, with very different rates depending on the μp kinetic energy being above or below the $2S$-$2P$ threshold ($\approx$0.3 eV in the lab frame) [9]. Most $\mu p(2S)$ atoms are formed at energies above this threshold [10], where collisional $2S \rightarrow 2P$ Stark transitions (followed by $2P \rightarrow 1S$ radiative deexcitation) lead to rather fast $2S$ depletion. This is the ''short-lived'' $2S$ component with a predicted lifetime [11] $\tau_{2S}^{\text{short}} \sim 100\ \text{ns}/p_{H_2}[\text{hPa}]$. There is, however, a competition between such Stark transitions and deceleration [9]. A fraction of the $\mu p(2S)$ atoms should therefore survive the process of slowing down below 0.3 eV, where transitions to the $2P$ state are energetically forbidden. These $\mu p(2S)$ atoms form the ''long-lived'' $2S$ component, with a lifetime τ_{2S}^{long} and a population $\varepsilon_{2S}^{\text{long}}$ (per μp atom).

The $2S$ population ε_{2S} is well determined from the measured μp x-ray yields [12–14]. $\varepsilon_{2S}^{\text{long}}$ can be derived from the measured $1S$ kinetic energy distributions [15] by using calculated elastic and inelastic $\mu p(2S)$ cross sections [9]. At 16 hPa, for example, $\varepsilon_{2S} = (4.40 \pm 0.17)\%$ and $\varepsilon_{2S}^{\text{long}} = (1.16 \pm 0.12)\%$. Calculations of the radiative quenching process *during* collisions [16–18] predicted values of $\tau_{2S}^{\text{long}} \sim 600$ ns or larger for a H_2 pressure of 64 hPa, but this could not be confirmed experimentally in searches for delayed $n = 2 \rightarrow 1$ x rays [12,19,20].

We report here on the first measurement of a nonradiative deexcitation mechanism for long-lived $\mu p(2S)$ atoms at gas pressures $p_{H_2} = 4$, 16, and 64 hPa at room temperature [15]. It was found in the analysis of time-of-flight (TOF) spectra which were measured to determine the $\mu p(1S)$ kinetic energy distributions at low densities. A pronounced fast component showed up, corresponding to a surprisingly high $\mu p(1S)$ kinetic energy of 0.9 keV.

The basic idea of the experiment is to form $\mu p(1S)$ atoms near the axis of a cylindrical gas target and to deduce their kinetic energy from the measured TOF they need to reach the gold-coated cylinder surface. The muon transfer reaction $\mu p + \text{Au} \rightarrow \mu\text{Au}^* + p$ to highly excited μAu^* takes place, and several μAu x rays with energies up to 9 MeV are emitted and detected by a CsI(Tl) scintillator. The cylindrical geometry gives a better kinetic energy resolution than earlier planar geometries [21].

Figure 1 shows the experimental setup. Negative muons with a momentum of $p = 10$ MeV/c from the high-intensity πE5 channel at PSI entered a 1 m long, 20 cm inner diameter solenoid operated at 5 T and evacuated to 10^{-5} hPa. Its fringe field reduced the radial beam size to a few mm in the region of full field. About 5000 μ^-/s reached a 16 μm thick Mylar entrance moderator. The muons were detected by a parallel-plate avalanche counter (PPAC) with a total areal density of 300 μg/cm^2. The PPAC is a double gas chamber filled with 16 hPa isobutane,

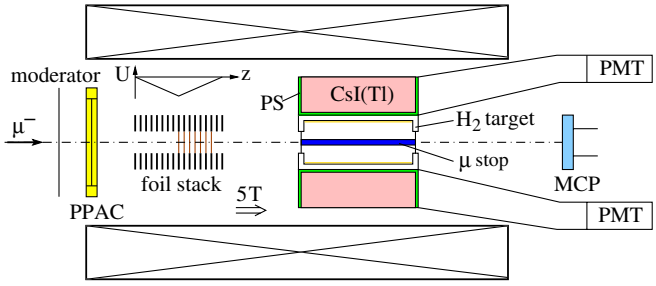

FIG. 1 (color online). Experimental setup inside the 5 T solenoid (not to scale, dimensions given in text). PS: plastic scintillator; PMT: photomultiplier tube. $U(z)$ is the electric potential of the 23 stack rings (7 with carbon foils).

with a detection efficiency up to 80%, depending on the muon energy. At the exit of the PPAC, the muons had energies between 0 and 200 keV. They then crossed a stack of seven thin carbon foils (each with an areal density of 5 μg/cm^2 and 2 cm diameter) where a few electrons were released. A high voltage applied to the stack ($\Delta U =$ 1800 V between successive foils) accelerated these electrons, and frictional cooling [22] enhanced the muon stop rate. After traversing the gas target, the electrons were detected in a microchannel plate (MCP). An incoming muon was identified by a delayed coincidence between the signals from PPAC and MCP. The muon detection efficiency of the stack-MCP assembly was ~40% for a target gas pressure of 4 hPa and decreased to ~15% at 64 hPa. The radial beam distribution was measured to be approximately Gaussian shaped with spreads $\sigma_x \approx \sigma_y \approx$ 1.8 mm in the 5 T field. The cyclotron radii of the muons were ~1 mm at 5 T.

The gas target vessel was a 26 cm long Al cylinder. Its inner cylindrical surface was coated with a 500 nm thick evaporated gold layer. The side walls were covered with polypropylene. Measurements were performed with two target inner radii, $R = 29$ and 10 mm. A target with polypropylene instead of gold was used to determine the background. Muon transfer to carbon does not produce x rays within the accepted μAu x-ray energy window.

The upstream and downstream target windows were thin Formvar foils (1 cm diameter) of 10 μg/cm^2 at $p_{H_2} = 4$ and 16 hPa, and 40 μg/cm^2 at 64 hPa. H_2 gas with <3 ppm impurities was continuously flushed through the target (exchange rate 2/ min). Outgassing from walls and pipes resulted in a total impurity concentration of order 10^{-4}. The measured μp formation rate was ~20 s^{-1}.

A 20 cm long cylindrical CsI(Tl) scintillator of 9.2 cm inner and 19 cm outer diameter was placed around the target. It had a high probability to detect at least one of the μAu x rays. The CsI(Tl) crystal was surrounded on all but the outer side by an 8 mm thick plastic scintillator acting as an anticoincidence detector against any charged particle background. The fast light component of the plastic scintillator was distinguished from the "slow" CsI light component (decay time ~1.5 μs) by pulse shape analysis.

For each incoming muon, the time difference between the MCP signal and a CsI signal from a μAu x ray was recorded. The true $\mu p(1S)$ TOF, however, starts at the formation of a $\mu p(1S)$. Time calibration measurements were done with a few percent of xenon admixed to the H_2 target gas, because at such a low Xe concentration μXe and μp formation times are nearly identical. The μXe x rays were detected in the CsI(Tl) crystal, too. Several Xe concentrations were used and the $\mu p(1S)$ formation time distribution was obtained by extrapolating to zero Xe concentration. A careful analysis of the μXe time spectra separated the time distribution of direct μXe formation from the (delayed) transfer reaction $\mu p + \mathrm{Xe} \rightarrow \mu\mathrm{Xe}^* + p$. Small residual deviations not taken into account by the Xe calibration (like the μp cascade time and discriminator threshold effects) were also considered.

Figure 2 shows the μAu time spectra measured at 64, 16, and 4 hPa for both target radii, and the μp formation time distributions deduced from the μXe data. The background was studied with the polypropylene target. It is dominated by bremsstrahlung from muon-decay electrons, with an additional component (depending on pressure) at times preceding μp formation, correlated to muons stopping in high-Z materials near the target. All μAu time spectra exhibit a wide distribution whose maximum corresponds to μp kinetic energies E_{kin} of 5 ... 20 eV. Such energies result from Coulomb deexcitations [23] $\mu p_n + H_2 \rightarrow \mu p_{n'<n} + E_{\mathrm{kin}} + p + \ldots$ during the cascade, a well-known effect for μp and πp atoms [9].

The data measured in the $R = 29$ mm target, which is most sensitive to high kinetic energies, show an unexpected peculiarity: The 64 hPa spectrum features an additional pronounced peak at $t \approx 100$ ns. This peak is also visible at 16 hPa, but almost disappears at 4 hPa. The corresponding kinetic energy is about 0.9 keV, indicated in Fig. 2 as a dotted line at 0.074 μs which is the calculated TOF for 29 mm.

Such a high-energy $\mu p(1S)$ component has never been reported before. It can only originate from radiationless deexcitation of $\mu p(n = 2)$ atoms in collisions with H_2 molecules. The $n = 2 \rightarrow 1$ transition energy of 1.9 keV is shared according to momentum conservation between the formed $\mu p(1S)$ and a proton of the H_2 molecule:

$$\mu p(n = 2) + H_2 \rightarrow \mu p_{1S}(0.9\ \mathrm{keV}) + p(1\ \mathrm{keV}) + \ldots .$$

A detailed analysis of the measured time spectra was performed using a set of Monte Carlo (MC) generated TOF spectra extending over the whole expected energy range (~10^{-2}–10^3 eV). In the MC, the target and detector geometries, axial and radial muon stop distributions, x-ray detection efficiencies, and scattering of μp atoms on H_2 molecules and on the gold surface of the target cylinder were taken into account [15]. Cross sections for $\mu p(1S) + H_2$ scattering calculated by Adamczak [24] for laboratory kinetic energies below 9 eV ($\approx H_2$ breakup energy) have been used. Between 9 and 1000 eV we applied those calculated by Cohen [25] for collisions with H atoms.

Coulomb deexcitation lines from low n levels were included in the fit function; the most important transitions are indicated in Fig. 2. A free fit gave only small amplitudes for Coulomb deexcitation components with $\Delta n > 1$, in accordance with calculations [23]. Finally, each MC TOF spectrum was convoluted with the measured μp formation time distribution. The fit function is a superposition of these spectra, with their individual weights treated as free parameters. For each pressure, the two time spectra measured for $R = 10$ and 29 mm were fitted simultaneously, providing a stringent consistency test because the two time spectra are very different for the same kinetic energy distribution.

An adequate fit of the data could not be obtained unless it was assumed that the 0.9 keV component was emitted with a nonzero lifetime. Such an effect can only be caused by long-lived $\mu p(2S)$ atoms. (Other collisional processes, like muon transfer to medium-Z atoms from gas impurities, would produce x rays with energies below those accepted for μAu.) For the data analysis a two-step process was adopted where the $\mu p(2S)$ atoms are first slowed down to low energies without significant quenching, and then collisionally quenched at a constant rate $\lambda_{2S}^{\text{quench}}$. The 0.9 keV MC time spectrum was therefore convoluted with an exponential, with lifetime $\tau_{2S}^{\text{long}} = (\lambda_{2S}^{\text{quench}} + \lambda_\mu)^{-1}$ and amplitude $A_{2S} = \varepsilon_{2S}^{\text{long}} \lambda_{2S}^{\text{quench}}$, delayed by a time offset Δt_{2S} for slowing down. ($\lambda_\mu = 4.55 \times 10^5\ \text{s}^{-1}$ is the muon-decay rate.)

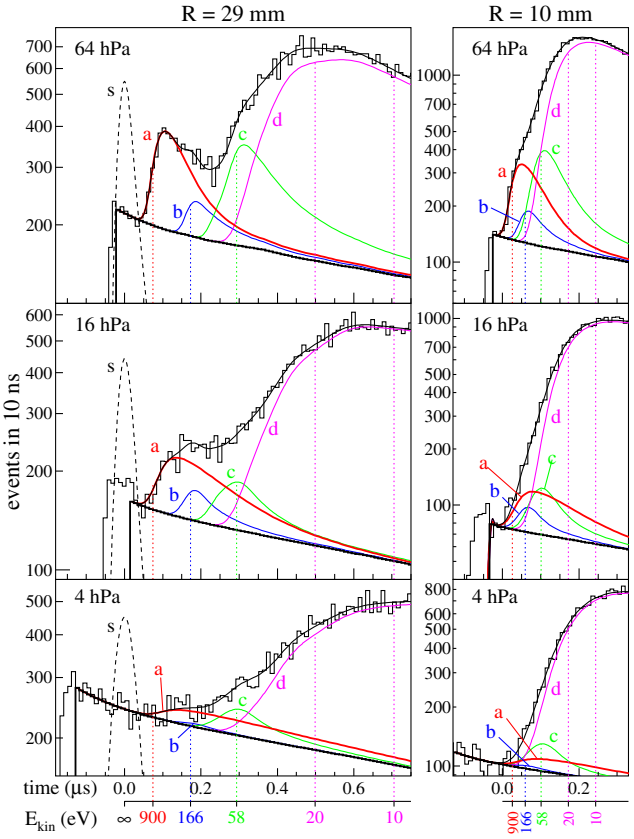

FIG. 2 (color online). Early part of the μAu time spectra measured at 64, 16, and 4 hPa (top to bottom) with the $R = 29$ mm (left) and $R = 10$ mm (right) targets. The corresponding μp kinetic energies are also indicated. Component (a) at 0.9 keV originates from nonradiative $\mu p(2S)$ quenching and was convoluted with the fitted $2S$ lifetime. The thin solid line is the total fit function, composed of the measured background (thick black line), the $2S$ component (a), the high-energy Coulomb deexcitation lines with main components (b) $n = 3 \rightarrow 2$ (166 eV) and (c) $n = 4 \rightarrow 3$ (58 eV), and a continuous distribution at energies below 60 eV (d). The dashed curve (labeled s) is the μp formation time distribution obtained in the Xe calibration measurements.

First the data sets at 64 and 16 hPa were analyzed independently of each other. (At 4 hPa the 0.9 keV component is too small to be treated in an independent fit.) Free fit parameters were the $2S$-quench time $\tau_{2S}^{\text{quench}} \equiv 1/\lambda_{2S}^{\text{quench}}$, the amplitude A_{2S}, the time offset Δt_{2S}, and the amplitudes of the Coulomb deexcitation components. The results are given in Table I. For Δt_{2S} a value of 8^{+18}_{-19} ns was obtained at 16 hPa, and roughly 4 times less at 64 hPa, i.e., much smaller than $\tau_{2S}^{\text{quench}}$.

Next, $\tau_{2S}^{\text{quench}}$ was set to be proportional to $1/p_{\text{H}_2}$, because nonlinear effects (like three-body collisions) can be excluded at our conditions. A combined fit of the data at all three pressures gave nearly the same values as the independent fit (Table I). The corresponding quench rate at room temperature is

$$\lambda_{2S}^{\text{quench}} = 5.1^{+2.4}_{-2.1} \times 10^5 \text{s}^{-1} \times p_{\text{H}_2}[\text{hPa}]$$

or, normalized to liquid-hydrogen atom density (LHD $= 4.25 \times 10^{22}$ atoms/cm^3),

$$\lambda_{2S}^{\text{quench}}(\text{LHD}) = 4.4^{+2.1}_{-1.8} \times 10^{11} \text{s}^{-1}. \quad (1)$$

The errors result from the quadratic sum of statistical and systematic errors. The combined fit gave a reduced χ^2 of 1.030 ($\chi^2 = 529.5$ for 514 degrees of freedom). $\chi^2 = 559.2$ resulted for $\tau_{2S}^{\text{quench}}$ (64 hPa) fixed to 9 ns, i.e., such a short $2S$ lifetime is statistically excluded at the 5σ confidence level.

TABLE I. $2S$ quench time $\tau_{2S}^{\text{quench}} = 1/\lambda_{2S}^{\text{quench}} (\approx \tau_{2S}^{\text{long}})$ and population $\varepsilon_{2S}^{\text{long}}$ (per μp atom) of the long-lived $\mu p(2S)$ component, obtained for the "independent" and "combined" fits of the time spectra. For the combined fit we give the statistical and the systematic errors, respectively. Only the statistical errors are given for the independent fits.

p_{H_2} (hPa)	Independent fit $\tau_{2S}^{\text{quench}}$ (ns)	Independent fit $\varepsilon_{2S}^{\text{long}}$ (%)	Combined fit $\tau_{2S}^{\text{quench}}$ (ns)	Combined fit $\varepsilon_{2S}^{\text{long}}$ (%)
64	30^{+23}_{-8}	$1.6^{+0.9}_{-0.3}$	$30.4^{+19.7+8.4}_{-7.3-6.3}$	$1.63^{+0.73+0.35}_{-0.20-0.15}$
16	124^{+542}_{-54}	$1.1^{+2.9}_{-0.4}$	4×	$1.07^{+0.41+0.16}_{-0.16-0.14}$
4			16×	$1.25^{+0.69+0.29}_{-0.25-0.23}$

Various sources of systematic errors were investigated: μp formation time, scattering on H_2 and gold, radial size of the muon stop distribution, and background shape. Uncertainties in the formation time gave a contribution of $^{+8.0}_{-4.7}$ ns to $\tau_{2S}^{\mathrm{quench}}$ (64 hPa), H_2-scattering one of $^{+1.0}_{-4.0}$ ns, whereas all other errors were considerably smaller. Gas impurities modified $\tau_{2S}^{\mathrm{quench}}$ (64 hPa) by <0.1 ns. The resulting total systematic errors are given in Table I.

The large value found for $\lambda_{2S}^{\mathrm{quench}}$ can be attributed to the formation of an *excited* muonic molecular ion in a resonantly enhanced reaction with H_2 [26,27]

$$\mu p(2S) + \mathrm{H}_2 \rightarrow \{[(pp\mu)^+]^* pee\}^*,$$

similar to the well-known formation of ground state muonic molecules in muon catalyzed fusion [28]. There is a series of resonant states just below the $\mu p(n = 2) + p$ dissociation limit [29]; rovibrational excitations of the electronic molecule absorb the small excess energy from the formation of the $(pp\mu)^+$ "pseudonucleus". A subsequent Auger decay to states with ≥ 16 eV binding energy stabilizes the $[(pp\mu)^+]^*$ against back decay. Mixing of the excited $[(pp\mu)^+]^*$ with the repulsive $(pp\mu)^+$ ground state finally leads to $\mu p(1S)$ atoms with 0.9 keV kinetic energy.

A theoretical estimate of the molecular formation rate [30] gave $\sim 5 \times 10^{10}$ s^{-1} at LHD, 10 times smaller than our result [Eq. (1)]. The calculation neglected the correlated motion of the three interacting atoms which is important in low-energy $\mu p(2S)$ collisions because of its long-range polarization potential. The triatomic molecule has a much denser vibrational-state spectrum with more ways to exchange excitation energy, leading to longer effective lifetimes of the compound system [31] and, correspondingly, higher molecular formation rates.

The populations $\varepsilon_{2S}^{\mathrm{long}}$ resulting at 16 and 4 hPa agree with the values of $(1.16 \pm 0.12)\%$ and $(1.03 \pm 0.09)\%$, respectively, evaluated for the $\mu p(2S)$ that slow down to below 0.3 eV [15]. This means that there is little room for radiative $2S \rightarrow 1S$ deexcitation processes and explains why no delayed 1.9 keV x rays were found in previous experiments [12,19,20]. The dominance of nonradiative $2S$ decay resulting from our measurements is in accord with recent calculations of the radiative and nonradiative decay rates of $[(pp\mu)^+]^*$ molecules [29,32].

In summary, we have measured that $\sim 1\%$ of all muons stopped in H_2 gas between 4 and 64 hPa form long-lived $\mu p(2S)$ atoms that decay nonradiatively into $\mu p(1S)$ atoms of 0.9 keV kinetic energy. For the current μp Lamb shift experiment, a pressure of ~ 1 hPa is needed where both the $2S$ population ($\sim 1\%$) and lifetime ($\tau_{2S}^{\mathrm{long}} = 1.04^{+0.29}_{-0.21}$ μs at 1 hPa) meet the experimental requirements [4]. First measurements at a new low-energy muon beam at PSI showed that enough μp atoms can be formed in a small gas volume at such pressures.

We thank G. Llosá and Ch. Maierl for their help during data taking; A. Adamczak, J. S. Cohen, and V. S. Melezhik for providing us with $\mu p(1S)$ scattering cross sections; T. Jensen, S. Romanov, and J. Wallenius for fruitful discussions; M. Aigner and H. Angerer for technical support; P. Maier-Komor and K. Nacke for manufacturing of ultrathin C foils; and the PSI staff for providing us with an excellent beam.

*Present address: MPI für Quantenoptik, Hans-Kopfermann-Str. 1 D-85748 Garching, Germany. Electronic address: Randolf.Pohl@mpq.mpg.de

[1] K. Pachucki, Phys. Rev. A **53**, 2092 (1996).
[2] M. I. Eides, H. Grotch, and V. A. Shelyuto, Phys. Rep. **342**, 63 (2001).
[3] E. Borie, Phys. Rev. A **71**, 032508 (2005).
[4] R. Pohl *et al.*, Can. J. Phys. **83**, 339 (2005).
[5] K. Pachucki, Phys. Rev. A **60**, 3593 (1999).
[6] B. de Beauvoir *et al.*, Eur. Phys. J. D **12**, 61 (2000).
[7] M. Niering *et al.*, Phys. Rev. Lett. **84**, 5496 (2000).
[8] P. J. Mohr and B. N. Taylor, Rev. Mod. Phys. **77**, 1 (2005).
[9] T. S. Jensen and V. E. Markushin, Eur. Phys. J. D **21**, 271 (2002).
[10] R. Pohl *et al.*, Hyperfine Interact. **127**, 161 (2000).
[11] G. Carboni and G. Fiorentini, Nuovo Cimento Soc. Ital. Fis. **39B**, 281 (1977).
[12] P. O. Egan *et al.*, Phys. Rev. A **23**, 1152 (1981).
[13] H. Anderhub *et al.*, Phys. Lett. B **143**, 65 (1984).
[14] M. Bregant *et al.*, Phys. Lett. A **241**, 344 (1998).
[15] R. Pohl, Ph.D. thesis 14096, ETH Zurich, 2001, available at http://e-collection.ethbib.ethz.ch/.
[16] R. O. Mueller, V. W. Hughes, H. Rosenthal, and C. S. Wu, Phys. Rev. A **11**, 1175 (1975).
[17] J. S. Cohen and J. N. Bardsley, Phys. Rev. A **23**, 46 (1981).
[18] L. I. Men'shikov and L. I. Ponomarev, Z. Phys. D **2**, 1 (1986).
[19] H. Anderhub *et al.*, Phys. Lett. B **71**, 443 (1977).
[20] J. A. Böcklin, Ph.D. thesis 7161, ETH Zurich, 1982.
[21] D. J. Abbott *et al.*, Phys. Rev. A **55**, 214 (1997).
[22] M. Mühlbauer *et al.*, Hyperfine Interact. **119**, 305 (1999).
[23] L. Bracci and G. Fiorentini, Nuovo Cimento Soc. Ital. Fis. **43A**, 9 (1978).
[24] A. Adamczak *et al.*, At. Data Nucl. Data Tables **62**, 255 (1996); (private communication).
[25] J. S. Cohen, Phys. Rev. A **43**, 4668 (1991); (private communication).
[26] P. Froelich and A. Flores-Riveros, Phys. Rev. Lett. **70**, 1595 (1993).
[27] J. Wallenius and P. Froelich, Phys. Rev. A **54**, 1171 (1996).
[28] A. Scrinzi *et al.*, Phys. Rev. A **47**, 4691 (1993).
[29] E. Lindroth, J. Wallenius, and S. Jonsell, Phys. Rev. A **68**, 032502 (2003); **69**, 059903(E) (2004).
[30] J. Wallenius, S. Jonsell, Y. Kino, and P. Froelich, Hyperfine Interact. **138**, 285 (2001).
[31] D. Taqqu, AIP Conf. Proc. **181**, 217 (1989).
[32] S. Kilic, J.-P. Karr, and L. Hilico, Phys. Rev. A **70**, 042506 (2004).